Title

Aqueous Electrochemical and pH Studies of Redox-Active Guanidino Functionalized Aromatics for CO2 Capture.

Journal

ACS Organic & Inorganic Au, 4(4)

Authors

Li, Clarabella

Ziller, Joseph

Barlow, Jeffrey

et al.

Publication Date

2024-08-07

DOI

10.1021/acsorginorgau.3c00066

Peer reviewed

ACS ORGANIC & INORGANIC Au
AN OPEN ACCESS JOURNAL OF THE AMERICAN CHEMICAL SOCIETY

pubs.acs.org/orginorgau
Article

Aqueous Electrochemical and pH Studies of Redox-Active Guanidino Functionalized Aromatics for CO_2 Capture

Published as part of ACS Organic & Inorganic Au virtual special issue "Electrochemical Explorations in Organic and Inorganic Chemistry".

Clarabella J. Li, Joseph W. Ziller, Jeffrey M. Barlow, and Jenny Y. Yang*

Cite This: ACS Org. Inorg. Au 2024, 4, 387−394
Read Online

ACCESS | Metrics & More | Article Recommendations | Supporting Information

ABSTRACT: Escalating levels of carbon dioxide (CO_2) in the atmosphere have motivated interest in CO_2 capture and concentration from dilute streams. A guanidino-functionalized aromatic 1,4-bis(tetramethylguanidino)benzene (1,4-btmgb) was evaluated both as a redox-active sorbent and as a pH swing mediator for electrochemical CO_2 capture and concentration. Spectroscopic and crystallographic studies demonstrate that 1,4-btmgb reacts with CO_2 in water to form 1,4-btmgb$H_2(HCO_3^-)_2$. The product suggests that 1,4-btmgb could be used in an aqueous redox pH swing cycle for the capture and concentration of CO_2. The synthesis and characterization of the mono- and diprotonated forms (1,4-btmgbH^+ and 1,4-btmgbH_2^{2+}) and their pK_a values were measured to be 13.5 and 11.0 in water, respectively. Electrochemical pH swing experiments indicate the formation of an intermediate radical species and other degradation pathways, which ultimately inhibited fully reversible redox-induced pH cycling.

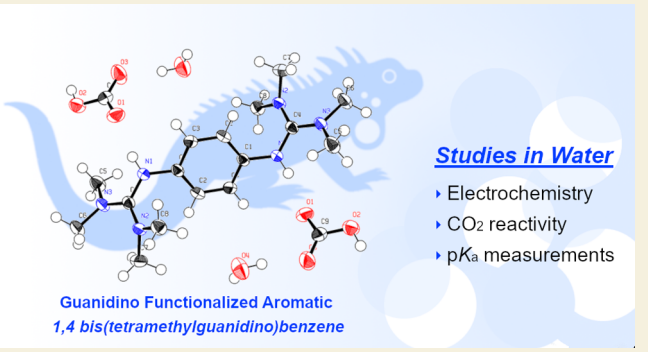

KEYWORDS: *electrochemistry, pH Swing, redox-active guanidine, CO_2 capture, electroswing*

Each year, about 40 gigatons of carbon dioxide is emitted from human activity, with roughly 30% of these emissions arising from fossil fuel power plants.[1,2] Flue gas from fossil fuel power plants typically contains 8−10% of CO_2. The current state-of-the-art method for the capture of CO_2 from flue gas uses an aqueous alkanolamine solution to capture CO_2 at ambient temperature and pressure. The release of CO_2 is achieved by heating the sorbent (383 K for monoethanolamine).[3,4] However, these thermal-swing methods can only achieve 5−40% of the maximum theoretical energy efficiency.[1,5]

Electrochemical methods can achieve greater theoretical energy efficiencies.[4,6] One common motif for ambient electrochemical CO_2 capture and concentration uses redox active molecules that either (1) directly bind to and release CO_2 or (2) modify the pH of aqueous solutions (Scheme 1A).[7] In the first approach, redox carriers bind CO_2 in their electron-rich reduced form (Scheme 1A, red pathway). Subsequent electrochemical oxidation decreases its electron density, lowering its CO_2 binding affinity and releasing concentrated CO_2. The redox carrier can then be regenerated for CO_2 capture via electrochemical reduction.[8] Another approach uses redox chemistry to change the pH of an aqueous solution for CO_2 capture and release (Scheme 1A, blue pathway). These pH swing cycles capitalize on pH-dependent CO_2 equilibria in aqueous solutions. At high pH values, hydroxide reacts with CO_2 to form bicarbonate and carbonate, enabling capture from dilute streams. At low pH values, the equilibrium is reversed and CO_2 is released. Redox-active molecules whose proton affinity (pK_a) significantly varies depending on their oxidation state are used to induce these electrochemically driven pH swings.[9]

Guanidines are a family of neutral organic Brønsted superbases (pK_a values of 12 or greater in water) with attractive CO_2 capture properties.[10] They bind CO_2 through two different mechanisms, depending on the solvent. These mechanisms parallel the two capture routes shown in Scheme 1A.[8] In aprotic solvents, tetramethyl guanidine (TMG) binds directly to CO_2 to form a zwitterionic carbamate salt (Scheme 1B, pathway A).[11] In protic solvents such as alcohols or water, sufficiently Brønsted basic guanidine deprotonates the alcohol

Received: December 14, 2023
Revised: February 27, 2024
Accepted: February 28, 2024
Published: March 22, 2024

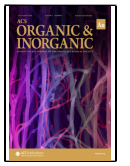

Scheme 1. Two Modes of CO_2Capture; A (Top): Two Modes of CO_2 Capture by a Redox-Active Molecule (R) via Direct Capture or pH Swing Methods; B (Bottom): Two Modes of CO_2 Capture by Guanidines

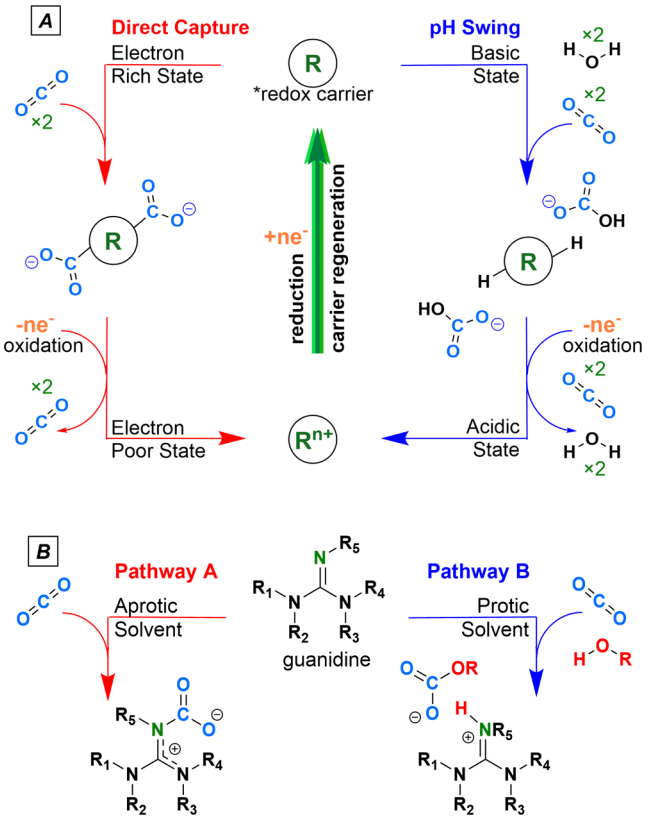

or water, which then binds CO_2 to form an alkyl carbonate or carbonate ion pair with the protonated TMG (Scheme 1B, pathway B).[12]

Because of their reactivity with CO_2, guanidine derivatives have been studied for their use in thermal capture and release cycles. Heldebrandt and co-workers developed a new class of CO_2-binding organic liquids composed of alcohol solvents and TMG derivatives.[12] Direct air capture (DAC) of CO_2 by a family of bis-iminoguanidine has been studied by Custelcean and co-workers.[13−15] The resulting bis-iminoguanidine carbamate salts can be heated to regenerate the sorbent (80−120 °C).[14,15]

The lack of reversible redox properties in the previously studied guanidine compounds limited their use as sorbents in thermal regeneration cycles. However, Himmel and co-workers recently synthesized TMG-substituted functionalized aromatics, or guanidino functionalized aromatics (GFAs), with reversible redox properties.[16] These redox-active superbases have not been assessed for electrochemical CO_2 capture and release. A variety of GFAs can be obtained through straightforward synthetic routes. Among these, 1,4-bis-(tetramethylguanidino)benzene (1,4-btmgb) was selected for testing due to its mild redox potential and stability in air. In this study, we explored the use of 1,4-btmgb in organic and aqueous solutions to assess its viability as a redox carrier and pH swing mediator for electrochemical CO_2 capture.

RESULTS AND DISCUSSION

Synthesis of GFAs

1,4-btmgb and the doubly oxidized form 1,4-btmgb$[BF_4]_2$ were synthesized as described by Himmel and co-workers (Scheme 2).[16] In addition, the previously unreported conjugate acids

Scheme 2. Synthesis of 1,4-btmgb, 1,4-btmgb^{2+}, and 1,4-btmgbH_2^{2+}

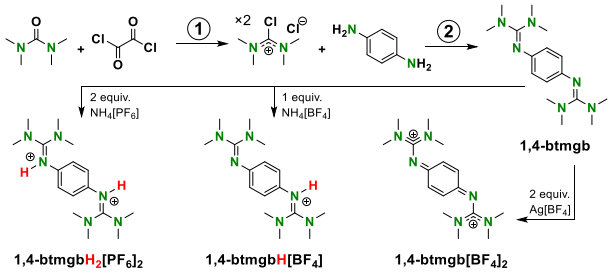

$[1,4\text{-btmgbH}_2]^{2+}$ with PF_6^- and Cl^- counteranions and monoprotonated $[1,4\text{-btmgbH}]^+$ with BF_4^- or PF_6^- counteranions were also synthesized. These protonated compounds were characterized via ^1H and $^{13}C\{^1H\}$ NMR spectroscopy (Figures S1−S3) and X-ray crystallography (Figures S4−S5).

pK_a and Electrochemical Properties in Acetonitrile

The pK_a values for the doubly protonated 1,4-btmgb, $[1,4\text{-btmgbH}_2]^{2+}$ were previously reported in acetonitrile (MeCN) as 19.3 and 22.1, respectively.[17] In MeCN, the cyclic voltammogram (CV) of the fully deprotonated 1,4-btmgb has a reversible two-electron oxidation with an $E_{1/2}$ at −0.25 V vs ferrocenium/ferrocene ($Fc^{+/0}$) (ΔE = 0.030 V) (Figure 1, top). This redox behavior is consistent with the previous reports of 1,4-btmgb in other organic solvents referenced to ferrocene, which described a reversible two-electron reduction at −0.18 V in DCM and −0.26 V in THF.[16]

The CV of the doubly protonated species, $[1,4\text{-btmgbH}_2]^{2+}$, is shown in Figure 1, bottom (and Figure S7). This species has irreversible oxidation events at the more anodic potentials of 1.12 and 1.39 V vs $Fc^{+/0}$. After oxidation, the subsequent reduction at −0.33 V is similar to the potential for the reduction of $[1,4\text{-btmgb}]^{2+}$ seen in the CV of deprotonated $[1,4\text{-btmgb}]^{2+}$/1,4-btmgb (Figure 1, top). Oxidation of $[1,4\text{-btmgbH}_2]^{2+}$ by two electrons is expected to result in an increase in acidity. We believe that $[1,4\text{-btmgbH}_2]^{4+}$ (formed upon the oxidation of $[1,4\text{-btmgbH}_2]^{2+}$) is deprotonated, despite the lack of an added base, to form the more stable 1,4-btmgb^{2+}. The CV trace for the monoprotonated species (Figure S8) maintains a one-electron redox couple centered at −0.24 V, a lone reduction event at 0.39 V, and oxidation peaks at 1.19 and 1.30 V vs $Fc^{+/0}$.

Reactivity with CO_2

The CO_2 capture capability of 1,4-btmgb was assessed in MeCN, with CO_2 being added to solutions of 1,4-btmgb under different conditions. Sparging CO_2 into a 1 mM solution of 1,4-btmgb in MeCN with trace water resulted in the formation of a white precipitate. Single crystals of this product, suitable for analysis by X-ray crystallography, were grown from a solution of concentrated 1,4-btmgb dissolved in MeCN under a CO_2 headspace. The analysis reveals the formation of protonated 1,4-btmgb with bicarbonate anions (1,4-$btmgbH_2(HCO_3^-)_2$) (Figure 2). Other attempts to recrystal-

https://doi.org/10.1021/acsorginorgau.3c00066
ACS Org. Inorg. Au 2024, 4, 387−394

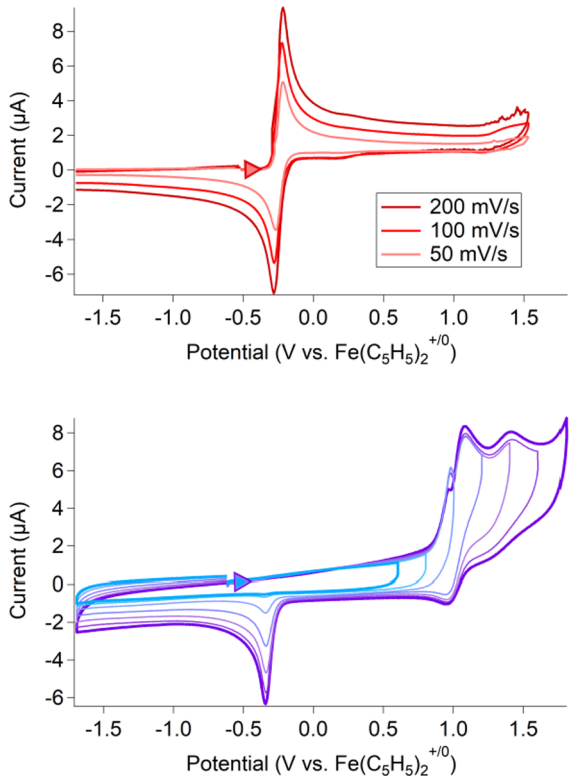

Figure 1. Top: 1,4-btmgb (1 mM) in MeCN with $TBAPF_6$ as the supporting electrolyte (100 mM) at varied scan rates. Bottom: varied scan window of 1,4-btmgb$H_2[PF_6]_2$ (scan rate = 500 mV/s) in MeCN, with 100 mM $TBAPF_6$ as the supporting electrolyte and a glassy carbon counter electrode. These and the following CVs were carried out at room temperature and are reported following the IUPAC convention.

lize 1,4-btmgb with CO_2 in MeCN resulted in a similar structure, but with two water molecules to give 1,4 btmgb$H_2(HCO_3^-)_2{\cdot}(H_2O)_2$ (Figure S6).

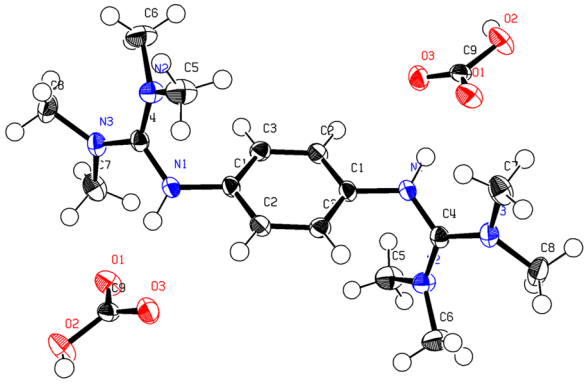

Figure 2. X-ray crystal structure of 1,4-btmgb$H_2(HCO_3^-)_2$. Thermal ellipsoids are shown at 80% probability. Refinement data can be found in SI Tables S1–S7.

The formation of a carbonate salt was also present in pure water, supported by ^1H NMR analysis. The ^1H NMR spectra of 1,4-btmgb in D_2O has signals at δ 6.85 and 2.82 ppm which shift to 7.11 and 2.97 ppm, respectively, after sparging with CO_2 for 5 min (Figures S9 and S10). After CO_2 exposure, these signals are identical to those found for doubly protonated 1,4-btmgb$H_2[PF_6]_2$ in D_2O (Figures S11 and S12). The $^{13}C\{^1H\}$ NMR of 1,4-btmgb in D_2O with added CO_2 is the same as that of 1,4-btmgb$H_2[PF_6]_2$ with two additional resonances observed at δ 124.8 and δ 160.3 ppm which correspond to dissolved free CO_2 in solution and bicarbonate (HCO_3^-), respectively.[18,19]

pK_a and Electrochemical Properties in Protic Solvents

Since even trace water in aprotic solvents results in the formation of the protonated base and bicarbonate, we postulate that 1,4-btmgb is a better candidate for an aqueous electrochemical pH swing cycle than direct capture. To assess the suitability of 1,4-btmgb for an aqueous electrochemical pH swing, we first sought to determine the pK_a values for $[1,4\text{-btmgbH}_2]^{2+}$ in water. Compared to the CVs obtained on 1,4-btmgb at various stages of protonation in MeCN (Figure 1), the CVs of 1,4-btmgb in water varied with pH (Figures 3 and

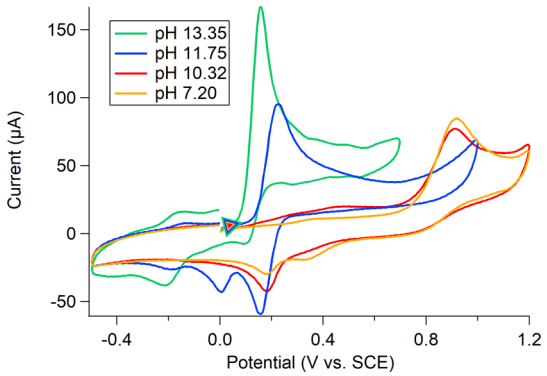

Figure 3. CVs of 1,4-btmgb in 100 mM KCl in H_2O at various pH values.

S15–S19), reflecting different protonation states. The relationship between the electrochemical potential and the solution pH with 1,4-btmgb was used to determine its pK_a values.[20−22] Cyclic voltammograms of 1,4-btmgb were acquired at pH values between 2.5 and 13.8. From these experiments, a partial Pourbaix diagram (Figure 4) was constructed by plotting the pH measured to the observed $E_{1/2}$ (or E_{pa} and E_{pc}, Figures S20–S22).[23] The reduction potential remained relatively

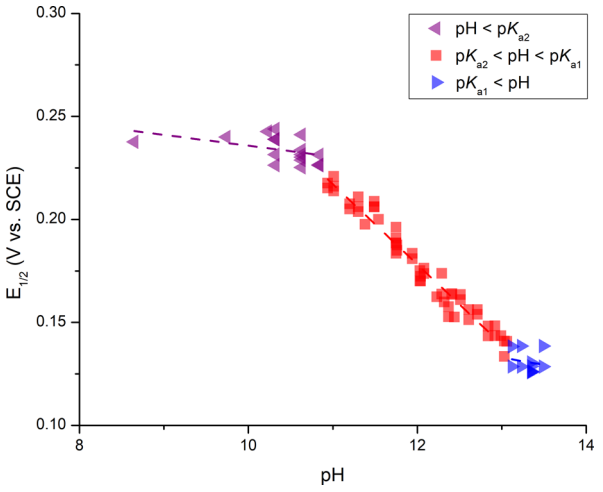

Figure 4. pH vs $E_{1/2}$ (V vs SCE) from points collected from titrating 1 M acetic acid and 1 M NaOH into 1,4-btmgb in aqueous KCl (conc.) solution.

https://doi.org/10.1021/acsorginorgau.3c00066
ACS Org. Inorg. Au 2024, 4, 387−394

constant below the pH value of 11. The oxidation potential shifted cathodically as the pH increased from 11 to 13.5 (Figures 4 and S20−S22). The slope of the shift in $E_{1/2}$ versus pH was observed to be −40.4 mV/pH, indicating a two-electron, one-proton process.[23] Above pH 13.5, there were minimal changes in the redox potential. Further supporting this, with differential-pulse voltammetry (DPV) experiments from pH 9.5 to 14.1, the exact breaking points in the pH-dependent and pH-independent regions allowed for the determination of pK_a values (Figures S23 and S24). Collectively, these data indicate a pK_{a1} value of approximately 13.5 ([1,4-btmgbH]$^+$) and a pK_{a2} value of 11.0 ([1,4-btmgbH$_2$]$^{2+}$).

The redox features of 1,4-btmgb are less reversible at both higher and lower pH values. Between pH 11.3−11.9 there were two additional reduction peaks negative of the reversible redox event at $E_{1/2}$ = 0.2 V vs saturated calomel electrode (SCE) (pH = 11.75) (Figure 3, blue trace). The reduction event at 0.0 V is attributed to the reduction of [1,4-btmgbH]$^{3+}$, from the oxidized [1,4 btmgbH]$^{1+}$ that is expected to form at these pH values. The more cathodic reduction event at −0.18 V vs SCE increases in current at high pH (11.3 and higher, Figure 3, green trace) but was not observed when 1,4-btmgb was probed electrochemically in other nonaqueous protic solvents (methanol and ethanol, Figures S25−S26). We attribute this reduction to an interaction with water upon oxidation, which is supported by electrolytic studies (vide infra).

Controlled Potential Electrolysis and Supporting Experiments

Electrochemically induced pH changes with 1,4-btmgb and [1,4-btmgbH$_2$][Cl$_2$] were attempted through controlled potential oxidative electrolysis in a divided H-cell. Two mM aqueous solutions of 1,4-btmgb were prepared. 1,4-btmgb is sufficiently basic to deprotonate water. As a result, the initial pH of the solution was 11.71 (±0.06). Controlled potential electrolysis was carried out at 0.5 V vs SCE to fully oxidize the [1,4-btmgbH]$^{1+}$ to [1,4-btmgbH]$^{3+}$ and [1,4-btmgb]$^{2+}$. The final pH was observed to be 9.50(±0.21).

An aqueous 2 mM solution of protonated [1,4-btmgbH$_2$]-[Cl$_2$] was also oxidized. The initial pH was 9.88 and then decreased to 8.72. Upon subsequent reduction, the pH of the solution increased to 9.38 (Table 1). While both solutions

Table 1. pH Values Observed before and after Electrolysis of 2 mM Solutions of 1,4-btmgb and 1,4-btmgbH$_2^{2+}$[a]

compound	initial pH	post oxidation	post reduction
1,4-btmgb	11.71 (±0.06)	9.50 (±0.21)	10.50
1,4-btmgbH$_2^{2+}$	9.88	8.72	9.38

[a]Electrolysis performed stirred in a divided H-cell, with a carbon fabric working electrode and SCE reference electrode on the working side and a glassy carbon electrode on the counter side. Further details of the electrolysis in the methods.

produced a change in pH from electrolysis, the magnitudes were smaller than expected and the solutions could not be restored to the original pH after reduction. The solutions also turned deep red during oxidation. The color faded in intensity over time but did not completely disappear. The CVs of the oxidized 1,4-btmgb solution are shown in Figure 5 (red trace). Compared to the trace of the solution before oxidation, a new reductive event appears at −0.18 V vs SCE. This feature and

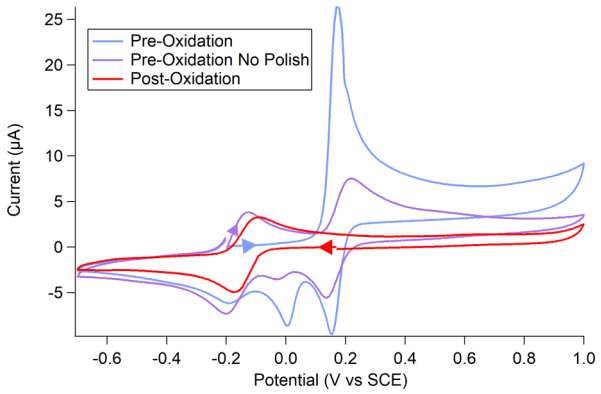

Figure 5. Two mM **1,4-btmgb** in 200 mM KCl and water, preoxidation scan rates 500 mV/s and postoxidation scan rate 250 mV/s.

the color change indicate the formation of new species after controlled potential oxidative electrolysis.

The redox event at −0.18 V vs SCE we attribute to an aniline species that is the product of the decomposition of 1,4-btmgb via the loss of a TMG group via base-catalyzed hydrolysis (Scheme 3). This reduction feature is present only

Scheme 3. Alkaline Hydrolysis of a TMG Group on Oxidized 1,4 btmgb

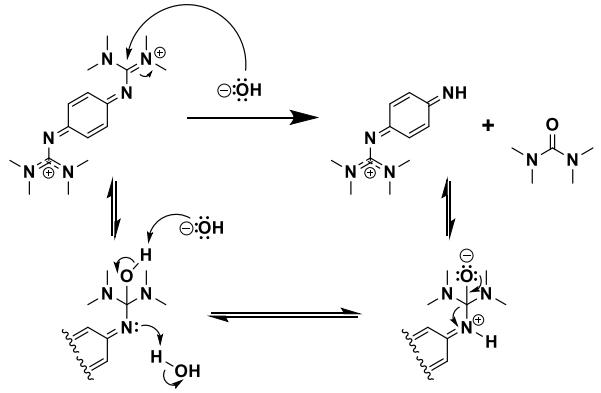

in CVs of 1,4-btmgb in water among the protic solvents surveyed, indicating it is related to the [1,4-btmgb^{2+}] generated in situ interacting with water/hydroxide. Prior studies have likened the redox behavior of the TMG substituted aniline to that of 1,4-bis(dimethylamino)-benzene where oxidation of this compound results in the Wurster cation and undergoes further decomposition in the solution mixture due to the N−H moiety.[24] There is literature precedence for this route of decomposition to form tetramethyl urea (Scheme 3).[25−27] ^{1}H NMR experiments were also performed on chemically oxidized [1,4-btmgb^{2+}] in deuterated acetonitrile in the presence of water, showing the decomposition of the parent species 30 min after the addition of water. Over the course of 5 h, additional resonances at around 2.89 ppm and in the aromatic region (6.74−6.76 ppm) increase in intensity (Figures S27 and S28). The resonance at 2.89 ppm is assigned to the methyl proton peaks of tetramethyl urea, and the resonances between 6.74−6.76 ppm are attributed to the aniline species formed post hydrolysis (tetramethylguanidino-dimethyl-*p*-phenylenediamine has aromatic resonances at 6.49−6.69 ppm while *p*-phenylenediamine has a resonance at 6.46 ppm in CD$_3$CN).[24]

https://doi.org/10.1021/acsorginorgau.3c00066
ACS Org. Inorg. Au 2024, 4, 387−394

Altogether, the new resonance peaks in the aromatic region indicate decomposition in the presence of water. Monitoring the reduced species 1,4-btmgb in D_2O at high and low pH via ^1H NMR spectroscopy does not show evidence of decomposition over the span of days, indicating it is the oxidized species that is sensitive to deleterious reactions with water.

Further evidence for decomposition with hydroxide upon oxidation is observed in the scan-rate dependent CVs. A new reductive feature appears after oxidation of $[1,4\text{-btmgbH}]^{3+}$ and the $[1,4\text{-btmgb}]^{2+}$ species (Figure S13). This reduction event at −0.18 V vs SCE increases with scan rates 250 mV/s and above and slower for solutions over pH 11.5 (Figures S13−S16). This reductive feature does not appear if the solution is not first oxidized.

In addition to the hydrolysis decomposition pathway in Scheme 3, we attribute the color change observed during electrolysis to a second decomposition pathway that results in radical formation. Prior studies in acetonitrile conditions have shown that the fully oxidized $[1,4\text{-btmgb}]^{2+}$ can comproportionate with 1,4-btmgb to form $[1,4\text{-btmgb}^{\cdot}]^{1+}$ in solution (Scheme 4).[28] Water is also known to stabilize this radical formation.[29]

Scheme 4. Various Proposed Comproportionation Pathways for $[1,4\text{-btmgb}]^{2+}$ (A) Unprotonated and (B) between a Reduced Monoprotonated Species $[1,4\text{-btmgbH}]^{+}$

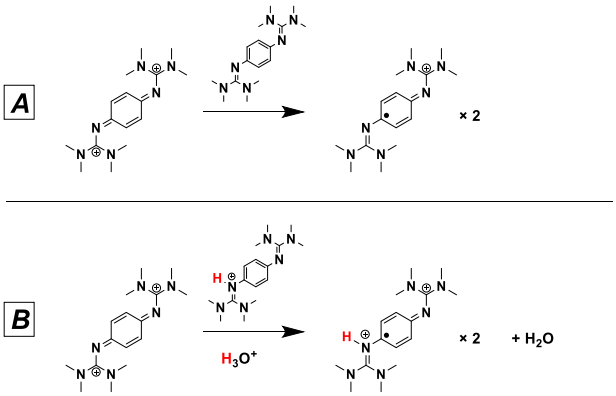

To verify the presence of a radical in the solution, electron paramagnetic resonance (EPR) spectra were acquired by using aliquots of the oxidized 2 mM 1,4-btmgb. An EPR signal at $g_\perp$ = 2.0066 was present for the solution after controlled potential electrolysis at 0.5 V for 10 min, indicating the formation of an S = 1/2 organic radical species (Figure S29).

Ultraviolet−visible (UV−vis) spectroelectrochemistry (SEC) was used to obtain absorption spectra of the generated oxidized species $[1,4\text{-btmgb}]^{2+}$ (Figure 6) through controlled potential electrolysis of a 0.1 mM solution of 1,4-btmgb with 100 mM KCl in water at 0.25 V vs SCE. $1,4\text{-btmgbH}^+$ has absorbances of 235 and 272 nm. Oxidation leads to two new absorbances at 224 and 291 nm, which have higher absorbance.

The postelectrolysis solution obtained after oxidation in an H-cell with stirring leads to different absorption spectra than what were observed in the UV−vis SEC experiments (Figure S30). The absorbances that correspond to the oxidized species were not present. We believe that convection increases the rate of comproportionation. After 1 day, the absorbance at 272 nm also decreases in intensity, indicating decomposition.

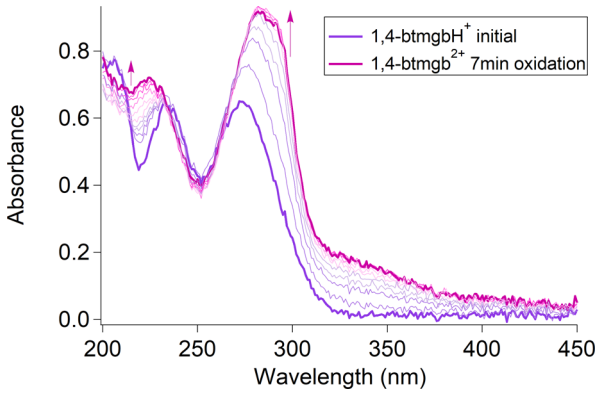

Figure 6. UV−visible spectroelectrochemical data of 0.1 mM 1,4-btmgb. Oxidation at 500 mV vs Ag^+/Ag electrode in unbuffered water with KCl (100 mM) was performed at pH 11.91. Under these conditions, it is expected to protonate once to give $1,4\text{-btmgbH}^+$. Purple trace is initial $1,4\text{-btmgbH}^+$ and pink trace is oxidized $1,4\text{-btmgb}^{2+}$ at 250 mV vs SCE.

The solubility of 1,4-btmgb was measured in water in the absence and presence of CO_2. Unlike MeCN, it was found that the addition of CO_2 does not diminish the solubility of 1,4-btmgb in water or lead to precipitation, even in saturated solutions. The determined solubility of 1,4-btmgb in water is 97 g/L (0.32 M) (Figures S31 and S32).

Collectively, these decomposition pathways result in smaller than expected pH changes in the controlled potential electrolysis experiments (Table 1). Additionally, the side reactions hinder the regeneration of 1,4-btmgb and the overall reversibility of an electrochemical cycle.

CONCLUSIONS

A guanidine-functionalized aromatic (GFA) compound, 1,4-btmgb, was examined as a redox-active candidate for CO_2 capture. Reactivity with CO_2 in the presence of trace water forms protonated guanidine and carbonate. In addition, the stability of 1,4-btmgb and the preliminary redox behavior in water indicate that it could potentially mediate a pH swing cycle. The aqueous pK_a values of $[1,4\text{-btmgbH}_2]^{2+}$ were measured to be 11.0 and 13.5. However, controlled potential electrolysis indicates more complicated reactivity in water with hydrolysis and radical formation decomposition pathways. The use of GFAs in electrochemical CO_2 capture and concentration will require addressing these decomposition pathways.

EXPERIMENTAL SECTION

General Information

Synthetic work was carried out in either ambient air or under a dinitrogen (N_2) atmosphere in a glovebox where noted. All solvents and reagents were purchased from commercial vendors and used without further purification unless otherwise noted. Deuterated acetonitrile used for NMR characterization were purchased from Cambridge Isotope Laboratories, Inc., and were degassed via free−pump−thaw and stored over activated 3 Å molecular sieves. Tetrabutylammonium hexafluorophosphate ($TBAPF_6$) was purified via recrystallization from ethanol and dried under a heated (80 °C) vacuum (1×10^{-3} Torr) and stored in a glovebox. Experiments using carbon dioxide (CO_2) atmospheres were performed using ultrahigh purity (99.999%) CO_2 which was additionally passed through a purification column to eliminate residual H_2O, O_2, CO, halocarbons, and sulfur compounds.

https://doi.org/10.1021/acsorginorgau.3c00066
ACS Org. Inorg. Au 2024, 4, 387−394

Electrochemical Methods

Electrochemical experiments were carried out under an atmosphere of N_2 or CO_2, where indicated. Solutions for electrochemical measurements were recorded in acetonitrile or water using 100 mM $TBAPF_6$ (or $TMAPF_6$) or 100 mM KCl as the supporting electrolytes, respectively. Cyclic voltammetry (CV) was performed with a Pine instrument WaveDriver 10 potentiostat. When specified, ferrocene (Fc) was used as an internal standard and potentials are referenced to the ferrocenium/ferrocene ($Fc^{+/0}$) couple. In water, a saturated calomel electrode (SCE) was used as the internal reference electrode. Between CV scan, the working electrode was polished in a figure eight pattern with an alumina slurry (0.05 um) on a microcloth (2.875 in, PSA backed). Controlled potential electrolysis experiments were performed stirred in a custom H-cell with the working and the counter cells divided by a porous glass frit. In the working compartment, carbon fabric was used as the working electrode and SCE as the reference. A glassy carbon rod was used as the counter electrode on the counter side cell. UV−visible spectroelectrochemistry (UV−vis SEC) was performed using a UV−vis SEC kit from Pine Instruments with a Pt working/counter electrode and Ag wire as a pseudo reference electrode.

Physical Methods

UV−vis absorption spectra were recorded by using a 1 cm quartz cuvette with an Agilent Cary 60 UV−vis spectrophotometer. CO_2 monitoring was performed on a CM-0111 gas sensor kit CM-0111 by CO_2Meter with the software GasLab. A Bruker EMX spectrometer equipped with an ER041XG microwave bridge was used to collect the X-band EPR spectra. Fourier Transform Infrared (FTIR) spectra were collected by using a Thermo Scientific Nicolet iS5 FTIR Spectrometer with iD5 diamond ATR. ^{1}H, $^{13}C\{^1H\}$, and $^{19}F\{^1H\}$ NMR spectra were recorded at 500 MHz on Bruker or 600 MHz Varian instruments. ^{1}H NMR spectra chemical shifts were reported as δ values in ppm relative to the residual solvent: D_2O (4.79 ppm), MeOD (3.31 ppm), and CD_3CN (1.94 ppm). pH values were collected with a Thermo Scientific Orion Star A216 pH/RDO/DO meter. The instrument was calibrated with Thermo Scientific buffers at pH 4.01, 7.00, and 10.01 each time before use.

X-ray diffraction studies were conducted at the UCI Department of Chemistry X-ray Crystallography Facility on a Bruker SMART APEX II or Bruker X8 Prospector diffractometer. Crystals were mounted in a cryoloop and transferred to a Bruker X8 Prospector (SMART APEX II, Mo Kα, λ = 0.71073 Å) or Bruker X8 Prospector (Cu Kα, λ = 1.5406 Å) diffractometer system. The APEX3[1] (APEX2[1]) program package was used to determine the unit-cell parameters and for data collection (2 s/frame scan time). The raw frame data was processed using SAINT[2] and SADABS[3] to yield the reflection data file. Subsequent calculations were carried out by using the SHELXTL[4] program package. There were no systematic absences nor any diffraction symmetry other than the Friedel condition. The structure was solved by direct methods and refined on F^2 by full-matrix least-squares techniques. The analytical scattering factors[5] for neutral atoms were used throughout the analysis. Hydrogen atoms were located from a difference-Fourier map and refined (x, y, z, and U_{iso}). The molecule was located about an inversion center.

1,4-Bis(tetramethylguanidino)benzene. Synthesized following previously described prep by Himmel and co-workers.[16] ^{1}H NMR (600 MHz, CD_3OD) δ = 6.63 (s, 4H) 2.72 (br, 24H) ppm. ^{1}H NMR (600 MHz, D_2O, unbuffered) δ = 6.85 (s, 4H), 2.82 (s, 24H) ppm. $^{13}C\{^1H\}$ (151 MHz, D_2O, unbuffered) δ = 161.2, 139.9, 122.5, 39.19 ppm.

1,4-btmgb[BF_4]$_2$. Synthesized following previously described prep by Himmel and co-workers, but using Ag[BF_4] instead of Ag[PF_6].[16] Use in water decomposition experiments in CD_3CN as seen in Figures S27 and S28.

1,4-btmgbH$_2$[PF_6]$_2$. In a glovebox, a mixture of 1,4-btmgb (0.018 g, 0.06 mmol) and [NH_4][PF_6] (0.016 g, 0.1 mmol) in dry MeCN (20 mL) was stirred for 45 min while heated at 55 °C. The solvent was removed under reduced pressure, and the resulting solid was redissolved in MeCN, yielding a clear yellow solution. Activated carbon was added, and the solution was left to stir for 15 min before being filtered through glass fiber. Removal of the solvent yielded a white powder that, when recrystallized from Et_2O, formed clear crystals. Yield: 14 mg (41%). ^{1}H NMR (600 MHz, CD_3CN) δ = 7.93 (s, 2H), 7.04 (s, 4H), 2.92 (s, 24H) ppm. (600 MHz, D_2O) δ = 7.11 (s, 4H), 2.97 (s, 24H) $^{13}C\{1H\}$ NMR (151 MHz, CD_3CN) δ = 159.3, 135.6, 123.3, 40.8 ppm. 13C{1H} (151 MHz, D_2O) δ = 158.6, 134.9, 122.3, 39.6 ppm. UV/vis (CH_3CN): λ_{max} (ε in L·(mol cm)$^{-1}$) = 277 (4.0 × 104), 231 (2.2 × 104) nm. FTIR (ATR)/cm^{-1} ν = 3400 (w), 3328 (w), 2926 (w), 1627 (m), 1563 (w), 1520 (w), 1466 (w), 1420 (m), 1316 (w), 1230 (w), 1165 (w), 1067 (w), 1041 (w), 917 (w), 822 (s), 741 (m), 557 (m). MS (ESI-MS) m/z calcd $C_{16}H_{29}N_6^+$ [M-H-2(PF_6)]$^+$ 305.25, found m/z 305.25. (Low-res MS) found m/z [M-PF_6]$^+$ 451.3, [M-H-$_2$(PF_6)]$^+$ 305.3, and [M/2]$^{2+}$ 153.2.

1,4-btmgbH$_2$[CO_3H]$_2$. Preparation varied, but for the general isolation of the compound, the procedure for characterization and experiments is as follows. A solution of 1,4-btmgb (10 mg) in MeCN (5 mL) was sparged with CO_2 for 3 min for CO_2 saturation at room temperature. While the solution was still actively sparged by CO_2, deionized water (0.1 mL) was added to the solution and a cloudy precipitate was observed to form. The solution was dried under a vacuum, yielding a chalky white power. Yield: quantitative. Crystals suitable for X-ray diffraction were grown from dissolved 1,4-btmgb in MeCN and drops of water, under a headspace of CO_2. ^{1}H NMR (600 MHz, CD_3OD) δ = 6.94 (s, 4H), 2.90 (s, 24H) ppm. ^{1}H NMR (600 MHz, D_2O) δ = 7.11 (s, 4H), 2.97 (s, 24H) ppm. $^{13}C\{^1H\}$ NMR (151 MHz, D_2O) δ: 160.3, 158.6, 134.9, 124.8, 122.3, 39.6 ppm. FTIR (ATR)/cm^{-1} v = 3380 (w), 3010 (w), 2917 (w), 2876 (w), 2802 (w), 2161 (w), 1564 (s), 1461 (s), 1437 (m), 1372 (s), 1268 (m), 1230 (m), 1204 (m), 1132 (s), 1097 (m), 1062 (w), 1016 (s), 922 (w), 841 (s), 751 (m), 685 (m), 638 (w), 578 (w). MS (ESI-MS) m/z calcd $C_{16}H_{29}N_6^+$ [M-H-2(CO_3H)]$^+$ 305.25, found m/z 305.25. (low-res MS) found m/z [M-H-2(CO_3H)]$^+$ 305.3, [M/2]$^{2+}$ 153.2.

1,4-btmgbH[BF_4]. In a glovebox, a mixture of 1,4-btmgb (0.021 g, 0.07 mmol) and [$NHBu_3$][BF_4] (0.019 g, 0.07 mmol) in dry MeCN (20 mL) was stirred for 1 h at 55 °C. The solvent was removed under reduced pressure, and the resulting beige solid was recrystallized from MeCN and Et_2O. Yield: 10 mg (50%). ^{1}H NMR (600 MHz, CD_3CN) δ = 7.79 (s, 1H), 6.73 (s, 4H), and 2.76 (s, 24H) ppm. $^{13}C\{^1H\}$ NMR (151 MHz, CD_3CN) δ = 159.1, 123.1, 122.3, 115.0, 39.4 ppm. $^{19}F\{^1H\}$ NMR (565 MHz, CD_3CN) δ = 151.8 ppm. FTIR (ATR)/cm^{-1} ν = 3382 (w), 3340 (w), 2932 (w), 2887 (w), 2361 (w), 2163 (w), 1630 (m), 1551 (m), 1493 (m), 1383 (m), 1318 (w), 1231 (w), 1205 (w), 1144 (w), 1049 (s), 1019 (s), 914 (w), 855 (m), 843 (m), 764 (w), 616 (w), 579 (w). MS (ESI-MS) m/z calcd $C_{16}H_{29}N_6^+$ [M-BF_4]$^+$ 305.25, found m/z 305.25.

■ ASSOCIATED CONTENT

Data Availability Statement

The data underlying this study are available in the published article and its Supporting Information.

Supporting Information

The Supporting Information is available free of charge at https://pubs.acs.org/doi/10.1021/acsorginorgau.3c00066.

In the order they are referenced in the main text, the SI contains characterization data (^{1}H, ^{13}C NMR, UV−vis, EPR, and FT-IR spectra), crystallographic structures and refinement data, additional CVs, and details of the DPV and pK_a determination experiments (PDF)

Accession Codes

CCDC 2314258−2314261 contain the supplementary crystallographic data for this paper. These data can be obtained free of charge via www.ccdc.cam.ac.uk/data_request/cif, or by emailing data_request@ccdc.cam.ac.uk, or by contacting The

https://doi.org/10.1021/acsorginorgau.3c00066
ACS Org. Inorg. Au 2024, 4, 387−394

Cambridge Crystallographic Data Centre, 12 Union Road, Cambridge CB2 1EZ, UK; fax: +44 1223 336033.

AUTHOR INFORMATION

Corresponding Author

Jenny Y. Yang − *Department of Chemistry, University of California, Irvine, Irvine, California 92697-2025, United States;* orcid.org/0000-0002-9680-8260; Email: j.yang@uci.edu

Authors

Clarabella J. Li − *Department of Chemistry, University of California, Irvine, Irvine, California 92697-2025, United States;* orcid.org/0000-0002-5551-4506

Joseph W. Ziller − *Department of Chemistry, University of California, Irvine, Irvine, California 92697-2025, United States;* orcid.org/0000-0001-7404-950X

Jeffrey M. Barlow − *Department of Chemistry, University of California, Irvine, Irvine, California 92697-2025, United States;* orcid.org/0000-0002-9536-8021

Complete contact information is available at: https://pubs.acs.org/10.1021/acsorginorgau.3c00066

Author Contributions

CRediT: **Clarabella J. Li** conceptualization, data curation, formal analysis, investigation, methodology, project administration, writing-original draft; **Joseph W. Ziller** data curation, formal analysis; **Jeffrey M. Barlow** conceptualization; **Jenny Y. Yang** conceptualization, formal analysis, funding acquisition, methodology, project administration, supervision, writing-review & editing.

Funding

Alfred P. Sloan Foundation, Research Corporation Scialog for Negative Emissions, Office of Naval Research through the National Oceanographic Partnership Program.

Notes

The authors declare no competing financial interest.

ACKNOWLEDGMENTS

This research was done with the support of the Alfred P. Sloan Foundation. C.J.L. would like to dedicate this work to Prof. Makhluf Haddadin from the University of Beirut, a collaborator and inspiration.

ABBREVIATIONS

btmgb, bis(tetramethylguanidino)benzene; CO_2, carbon dioxide; CV, cyclic voltammetry; DAC, direct air capture; DPV, differential-pulse voltammetry; EPR, electron paramagnetic resonance; GFA, guanidino functionalized aromatics; SCE, saturated calomel electrode; TMG, tetramethyl guanidine.

REFERENCES

(1) Aaron, D.; Tsouris, C. Separation of CO2 from Flue Gas: A Review. *Sep. Sci. Technol.* **2005**, *40* (1−3), 321−348.

(2) Friedlingstein, P.; O'Sullivan, M.; Jones, M. W.; Andrew, R. M.; Bakker, D. C. E.; Hauck, J.; Landschützer, P.; Le Quéré, C.; Luijkx, I. T.; Peters, G. P.; Peters, W.; Pongratz, J.; Schwingshackl, C.; Sitch, S.; Canadell, J. G.; Ciais, P.; Jackson, R. B.; Alin, S. R.; Anthoni, P.; Barbero, L.; Bates, N. R.; Becker, M.; Bellouin, N.; Decharme, B.; Bopp, L.; Brasika, I. B. M.; Cadule, P.; Chamberlain, M. A.; Chandra, N.; Chau, T.-T.-T.; Chevallier, F.; Chini, L. P.; Cronin, M.; Dou, X.; Enyo, K.; Evans, W.; Falk, S.; Feely, R. A.; Feng, L.; Ford, D. J.; Gasser, T.; Ghattas, J.; Gkritzalis, T.; Grassi, G.; Gregor, L.; Gruber, N.; Gürses, Ö.; Harris, I.; Hefner, M.; Heinke, J.; Houghton, R. A.; Hurtt, G. C.; Iida, Y.; Ilyina, T.; Jacobson, A. R.; Jain, A.; Jarníková, T.; Jersild, A.; Jiang, F.; Jin, Z.; Joos, F.; Kato, E.; Keeling, R. F.; Kennedy, D.; Klein Goldewijk, K.; Knauer, J.; Korsbakken, J. I.; Körtzinger, A.; Lan, X.; Lefèvre, N.; Li, H.; Liu, J.; Liu, Z.; Ma, L.; Marland, G.; Mayot, N.; McGuire, P. C.; McKinley, G. A.; Meyer, G.; Morgan, E. J.; Munro, D. R.; Nakaoka, S.-I.; Niwa, Y.; O'Brien, K. M.; Olsen, A.; Omar, A. M.; Ono, T.; Paulsen, M.; Pierrot, D.; Pocock, K.; Poulter, B.; Powis, C. M.; Rehder, G.; Resplandy, L.; Robertson, E.; Rödenbeck, C.; Rosan, T. M.; Schwinger, J.; Séférian, R.; Smallman, T. L.; Smith, S. M.; Sospedra-Alfonso, R.; Sun, Q.; Sutton, A. J.; Sweeney, C.; Takao, S.; Tans, P. P.; Tian, H.; Tilbrook, B.; Tsujino, H.; Tubiello, F.; van der Werf, G. R.; van Ooijen, E.; Wanninkhof, R.; Watanabe, M.; Wimart-Rousseau, C.; Yang, D.; Yang, X.; Yuan, W.; Yue, X.; Zaehle, S.; Zeng, J.; Zheng, B. Global Carbon Budget 2023. *Earth Syst. Sci. Data* **2023**, *15* (12), 5301−5369.

(3) Davis, J.; Rochelle, G. Thermal Degradation of Monoethanolamine at Stripper Conditions. *Energy Procedia* **2009**, *1* (1), 327−333.

(4) Zito, A. M.; Clarke, L. E.; Barlow, J. M.; Bím, D.; Zhang, Z.; Ripley, K. M.; Li, C. J.; Kummeth, A.; Leonard, M. E.; Alexandrova, A. N.; Brushett, F. R.; Yang, J. Y. Electrochemical Carbon Dioxide Capture and Concentration. *Chem. Rev.* **2023**, *123* (13), 8069−8098.

(5) House, K. Z.; Harvey, C. F.; Aziz, M. J.; Schrag, D. P. The Energy Penalty of Post-Combustion CO2 Capture & Storage and Its Implications for Retrofitting the U.S. Installed Base. *Energy Environ. Sci.* **2009**, *2* (2), 193−205.

(6) Clarke, L. E.; Leonard, M. E.; Hatton, T. A.; Brushett, F. R. Thermodynamic Modeling of CO2 Separation Systems with Soluble, Redox-Active Capture Species. *Ind. Eng. Chem. Res.* **2022**, *61* (29), 10531−10546.

(7) Barlow, J. M.; Clarke, L. E.; Zhang, Z.; Bím, D.; Ripley, K. M.; Zito, A.; Brushett, F. R.; Alexandrova, A. N.; Yang, J. Y. Molecular Design of Redox Carriers for Electrochemical CO2 Capture and Concentration. *Chem. Soc. Rev.* **2022**, *51* (20), 8415−8433.

(8) Rheinhardt, J. H.; Singh, P.; Tarakeshwar, P.; Buttry, D. A. Electrochemical Capture and Release of Carbon Dioxide. *ACS Energy Lett.* **2017**, *2* (2), 454−461.

(9) Jin, S.; Wu, M.; Gordon, R. G.; Aziz, M. J.; Kwabi, D. G. pH Swing Cycle for CO_2 Capture Electrochemically Driven through Proton-Coupled Electron Transfer. *Energy Environ. Sci.* **2020**, *13* (10), 3706−3722.

(10) Puleo, T. R.; Sujansky, S. J.; Wright, S. E.; Bandar, J. S. Organic Superbases in Recent Synthetic Methodology Research. *Chem. − Eur. J.* **2021**, *27* (13), 4216−4229.

(11) Pereira, F. S.; deAzevedo, E. R.; da Silva, E. F.; Bonagamba, T. J.; da Silva Agostíni, D. L.; Magalhães, A.; Job, A. E.; Pérez González, E. R. Study of the Carbon Dioxide Chemical Fixation—Activation by Guanidines. *Tetrahedron* **2008**, *64* (43), 10097−10106.

(12) Heldebrant, D. J.; Yonker, C. R.; Jessop, P. G.; Phan, L. Organic Liquid CO2 Capture Agents with High Gravimetric CO2 Capacity. *Energy Environ. Sci.* **2008**, *1* (4), 487−493.

(13) Seipp, C. A.; Williams, N. J.; Kidder, M. K.; Custelcean, R. CO2 Capture from Ambient Air by Crystallization with a Guanidine Sorbent. *Angew. Chem., Int. Ed.* **2017**, *56* (4), 1042−1045.

(14) Custelcean, R.; Williams, N. J.; Garrabrant, K. A.; Agullo, P.; Brethomé, F. M.; Martin, H. J.; Kidder, M. K. Direct Air Capture of CO2 with Aqueous Amino Acids and Solid Bis-Iminoguanidines (BIGs). *Ind. Eng. Chem. Res.* **2019**, *58* (51), 23338−23346.

(15) Kasturi, A.; Gabitto, J.; Tsouris, C.; Custelcean, R. Carbon Dioxide Capture with Aqueous Amino Acids: Mechanistic Study of Amino Acid Regeneration by Guanidine Crystallization and Process Intensification. *Sep. Purif. Technol.* **2021**, *271*, No. 118839.

(16) Hornung, J.; Hübner, O.; Kaifer, E.; Himmel, H.-J. Bent and Twisted: The Electronic Structure of 2-Azapropenylium Ions Obtained by Guanidine Oxidation. *RSC Adv.* **2016**, *6* (45), 39323−39329.

(17) Leffek, K. T.; Pruszynski, P.; Thanapaalasingham, K. Basicity of Substituted 2-Phenyl-1,1,3,3- Tetramethylguanidines and Other Bases in Acetonitrile Solvent. *Can. J. Chem.* **1989**, *67* (4), 590−595.
(18) Perinu, C.; Arstad, B.; Jens, K.-J. NMR Spectroscopy Applied to Amine−CO2−H2O Systems Relevant for Post-Combustion CO2 Capture: A Review. *Int. J. Greenh. Gas Control* **2014**, *20*, 230−243.
(19) Surface, J. In Situ High Pressure and Temperature 13C NMR for the Study of Carbonation Reactions of CO2. Theses Diss, ETDs, 2013.
(20) Harriman, A. Further Comments on the Redox Potentials of Tryptophan and Tyrosine. *J. Phys. Chem.* **1987**, *91* (24), 6102−6104.
(21) Sjödin, M.; Styring, S.; Wolpher, H.; Xu, Y.; Sun, L.; Hammarström, L. Switching the Redox Mechanism: Models for Proton-Coupled Electron Transfer from Tyrosine and Tryptophan. *J. Am. Chem. Soc.* **2005**, *127* (11), 3855−3863.
(22) Tyburski, R.; Liu, T.; Glover, S. D.; Hammarström, L. Proton-Coupled Electron Transfer Guidelines, Fair and Square. *J. Am. Chem. Soc.* **2021**, *143* (2), 560−576.
(23) Zanello, P. *Inorganic Electrochemistry: Theory, Practice and Application*; The Royal Society of Chemistry: Cambridge: University of Siena, Italy, 2003.
(24) Walter, P.; Kaifer, E.; Herrmann, H.; Wadepohl, H.; Hübner, O.; Himmel, H.-J. Redox-Active Guanidines with One or Two Guanidino Groups and Their Integration in Low-Dimensional Perovskite Structures. *Eur. J. Inorg. Chem.* **2019**, *2019* (38), 4147−4160.
(25) Homer, R. B.; Alwis, K. W. Kinetics and Mechanism of the Alkaline Hydrolysis of Guanidine, Hexamethylguanidinium Perchlorate, and Tetramethylurea. *J. Chem. Soc. Perkin Trans. 2* **1976**, *7*, 781−784.
(26) Limatibul, S.; Watson, J. The Mechanism of Acid Hydrolysis of Guanidines. *J. Org. Chem.* **1971**, *36* (24), 3805−3807.
(27) Lewis, C. A., Jr.; Wolfenden, R. The Nonenzymatic Decomposition of Guanidines and Amidines. *J. Am. Chem. Soc.* **2014**, *136* (1), 130−136.
(28) Wild, U.; Walter, P.; Hübner, O.; Kaifer, E.; Himmel, H.-J. Evaluation of the Synthetic Scope and the Reaction Pathways of Proton-Coupled Electron Transfer with Redox-Active Guanidines in C−H Activation Processes. *Chem. − Eur. J.* **2020**, *26* (69), 16504−16513.
(29) Yorimitsu, H.; Nakamura, T.; Shinokubo, H.; Oshima, K.; Omoto, K.; Fujimoto, H. Powerful Solvent Effect of Water in Radical Reaction: Triethylborane-Induced Atom-Transfer Radical Cyclization in Water. *J. Am. Chem. Soc.* **2000**, *122* (45), 11041−11047.

https://doi.org/10.1021/acsorginorgau.3c00066
ACS Org. Inorg. Au 2024, 4, 387−394